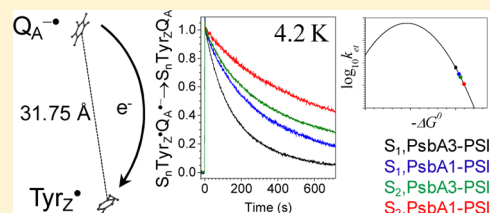


# Charge Recombination in $S_n\text{Tyr}_Z^{\bullet}\text{Q}_A^{-\bullet}$ Radical Pairs in D1 Protein Variants of Photosystem II: Long Range Electron Transfer in the Marcus Inverted Region

Alain Boussac,<sup>\*,†</sup> Fabrice Rappaport,<sup>‡</sup> Klaus Brettel,<sup>†</sup> and Miwa Sugiura<sup>§</sup><sup>†</sup>iBiTec-S, CNRS UMR 8221, CEA Saclay, 91191 Gif-sur-Yvette, France<sup>‡</sup>Institut de Biologie Physico-Chimique, CNRS UMR 7141 and Université Pierre et Marie Curie, 13 rue Pierre et Marie Curie, 75005 Paris, France<sup>§</sup>Proteo-Science Research Center, Ehime University, Bunkyo-cho, Matsuyama, Ehime 790-8577, Japan

## Supporting Information

**ABSTRACT:** Charge recombination in the light-induced radical pair  $S_n\text{Tyr}_Z^{\bullet}\text{Q}_A^{-\bullet}$  in Photosystem II (PSII) from *Thermosynechococcus elongatus* has been studied at cryogenic temperatures by time-resolved EPR for different configurations of PSII that are expected to affect the driving force of the reaction (oxidation states  $S_0$ ,  $S_1$ , or  $S_2$  of the  $\text{Mn}_4\text{CaO}_5$  cluster; PsbA1, PsbA2, or PsbA3 as D1 protein). The kinetics were independent of temperature in the studied range from 4.2 to 50 K and were not affected by exchange of  $\text{H}_2\text{O}$  for  $\text{D}_2\text{O}$ , consistent with single-step electron tunneling over the distance of  $\sim 32$  Å without any repopulation through Boltzmann equilibration of intermediates lying higher in energy. In PsbA1-PSII, the charge recombinations in the radical pairs  $S_n\text{Tyr}_Z^{\bullet}\text{Q}_A^{-\bullet}$  ( $k_{\text{et}} = 3.4 \times 10^{-3} \text{ s}^{-1}$  for  $S_1$ ) were slower than in PsbA3-PSII despite an expected lower driving force owing to a downshifted  $E_m(\text{Q}_A/\text{Q}_A^{-\bullet})$  in PsbA1-PSII. Conversely, the reaction was slower in the presence of  $S_2$  than in the presence of  $S_1$ , despite an expected larger driving force due to an upshifted  $E_m(\text{Tyr}_Z^{\bullet}/\text{Tyr}_Z)$  in  $S_2$ . These observations indicate that the charge recombination occurs in the Marcus inverted region. Assuming that the driving force of the reaction ( $-\Delta G^0 \approx 1.2 \text{ eV}$  at room temperature for  $S_1$ ) does not vary strongly with temperature, the data indicate an optimal electron transfer rate (for a hypothetical  $-\Delta G^0 = \lambda$ ) substantially faster than would be predicted from extrapolation of room temperature intraprotein ET rates over shorter distances. Possible origins of this deviation are discussed, including a possible enhancement of the electronic coupling of  $\text{Tyr}_Z^{\bullet}$  and  $\text{Q}_A^{-\bullet}$  by aromatic cofactors located in between. Observed similar  $S_1\text{Tyr}_Z^{\bullet}\text{Q}_A^{-\bullet}$  charge recombinations in PsbA2-PSII and PsbA3-PSII predict that  $E_m(\text{Q}_A/\text{Q}_A^{-\bullet})$  in PsbA2-PSII is similar to that in PsbA3-PSII.



## INTRODUCTION

The light-driven oxidation of water in PSII is the first step in the photosynthetic production of biomass, fossil fuels, and  $\text{O}_2$  on Earth. PSII is made up of 17 membrane protein subunits and 3 extrinsic proteins. Altogether, these bear 35 chlorophylls, 2 pheophytins (Phe), 2 hemes, 1 nonheme iron, 2 plastoquinones ( $\text{Q}_A$  and  $\text{Q}_B$ ), 4 Mn ions, 1  $\text{Ca}^{2+}$ , 2  $\text{Cl}^-$ , 12 carotenoids, and 25 lipids.<sup>1</sup> The excitation resulting from the absorption of a photon is transferred to the photochemical trap that undergoes charge separation. The positive charge is then stabilized on  $\text{P}_{680}$ , a weakly coupled chlorophyll dimer. Then,  $\text{P}_{680}^{+\bullet}$  oxidizes  $\text{Tyr}_Z$ , the Tyr161 of the D1 polypeptide, which in turn oxidizes the  $\text{Mn}_4\text{CaO}_5$  cluster. On the electron acceptor side, the electron is transferred to the primary quinone electron acceptor,  $\text{Q}_A$ , and then to  $\text{Q}_B$ , a two-electron and two-proton acceptor, for example.<sup>2–7</sup> The  $\text{Mn}_4\text{CaO}_5$  cluster both accumulates oxidizing equivalents and acts as the catalytic site for water oxidation. The enzyme cycles sequentially through five redox states, denoted  $S_n$ , where  $n$  stands for the number of stored oxidizing equivalents. Upon formation of the  $S_4$  state

two molecules of water are rapidly oxidized, the  $S_0$  state is regenerated and  $\text{O}_2$  released.<sup>8,9</sup>

Cyanobacteria bear 3 to 6 *psbA* genes encoding the D1 protein (also noted PsbA), for example,<sup>10</sup> *Thermosynechococcus elongatus* has 3 *psbA* genes and among the 344 residues of the PsbA proteins, 21 differ between PsbA1 and PsbA3, 31 between PsbA1 and PsbA2, and 27 between PsbA2 and PsbA3.<sup>11</sup> The midpoint potential  $E_m(\text{Q}_A/\text{Q}_A^{-\bullet})$  is upshifted by  $\approx 38 \text{ mV}$  upon the exchange of PsbA1 by PsbA3,<sup>12</sup> whereas the  $E_m(\text{Tyr}_Z^{\bullet}/\text{Tyr}_Z)$  appeared not to be modified because both the oxidation of  $\text{Tyr}_Z$  by  $\text{P}_{680}^{+\bullet}$  and the reduction of  $\text{Tyr}_Z^{\bullet}$  by the  $\text{Mn}_4\text{CaO}_5$  cluster remained unaffected by the PsbA1/PsbA3 exchange.<sup>13,14</sup>

In PsbA2-PSII, it has been recently proposed that the geometry of the  $\text{Tyr-O}\cdots\text{H}\cdots\text{N}\varepsilon\text{-His}$  bonding is slightly modified when compared to PsbA(1/3)-PSII in the  $S_2$  state, whereas in the  $S_1$  state the  $\text{Tyr}_Z$  oxidation by  $\text{P}_{680}^{+\bullet}$  and the  $\text{Tyr}_Z^{\bullet}$  reduction by the  $\text{Mn}_4\text{CaO}_5$  cluster remained almost

Received: January 11, 2013

Revised: February 16, 2013

unaffected.<sup>15</sup> The properties of PsbA2-PSII are however much less documented than those of PsbA1-PSII and PsbA3-PSII and the  $E_m(Q_A/Q_A^{\bullet-})$  value has not yet been determined in this PSII variant.

Illumination at liquid helium temperatures of PSII, previously trapped at room temperature in the  $S_0$ ,  $S_1$ , and  $S_2$  states, induces the formation of the  $S_0\text{Tyr}_Z^{\bullet}Q_A^{\bullet-}$ ,  $S_1\text{Tyr}_Z^{\bullet}Q_A^{\bullet-}$ , and  $S_2\text{Tyr}_Z^{\bullet}Q_A^{\bullet-}$  states, respectively.<sup>16–19</sup> Each of the three  $S_n\text{Tyr}_Z^{\bullet}$  states give rise to distinct and characteristic split EPR signals,<sup>16–19</sup> making them unambiguously identifiable (see also Figure S1). These signals are interpreted as resulting from the magnetic interaction between  $\text{Tyr}_Z^{\bullet}$ , with a spin state  $S = 1/2$  and the  $\text{Mn}_4\text{CaO}_5$  cluster. As they lie higher in energy than the ground state, the  $S_n\text{Tyr}_Z^{\bullet}Q_A^{\bullet-}$  states are not stable and decay by charge recombination, for example,<sup>20,21</sup> back to the  $S_n\text{Tyr}_ZQ_A$  states (see also Figure S2). The kinetics of the charge recombinations depend on their driving force or, in other terms, on  $E_m(Q_A/Q_A^{\bullet-})$  and  $E_m(\text{Tyr}_Z^{\bullet}/\text{Tyr}_Z)$ .

According to Marcus theory,<sup>22,23</sup> the rate  $k_{\text{et}}$  of nonadiabatic electron transfer (ET) for weakly coupled pairs ( $A^{\bullet-}B \rightarrow AB^{\bullet-}$ ) can be expressed as  $k_{\text{et}} = (2\pi/\hbar)H_{\text{AB}}^2[1/(4\pi\lambda k_B T)^{1/2}] \exp\{-[(\Delta G^0 + \lambda)^2]/[4\lambda k_B T]\}$ , where  $\Delta G^0$  is the standard free reaction energy (i.e.,  $-\Delta G^0$  is the driving force),  $\lambda$  is the reorganization energy,  $T$  is the temperature,  $k_B$  is the Boltzmann constant, and  $H_{\text{AB}}$  is the electronic coupling between the donor and the acceptor. At low temperatures, this semiclassical expression, when nuclear motions were treated classically, whereas the electron is allowed to tunnel through the potential barrier, predicts a dramatic drop of the ET rate (except for the special case:  $-\Delta G^0 = \lambda$ ) because the exponential term decreases much more steeply than the rise of the pre-exponential term.

Later on, nuclear motions were treated by quantum mechanics. For a single high frequency vibrational mode  $\omega$  coupled to ET, Hopfield<sup>24</sup> derived the expression  $k_{\text{et}} = (2\pi/\hbar)H_{\text{AB}}^2 \times [1/(2\lambda\pi\hbar\omega \coth(\hbar\omega/2k_B T))^{1/2}] \exp[-(\Delta G^0 + \lambda)^2/2\lambda\hbar\omega \coth(\hbar\omega/2k_B T)]$ . The ET rate is now virtually temperature independent, but not zero, as soon as  $k_B T \ll \hbar\omega$  (nuclear tunneling).

A remarkable feature already evidenced by Marcus theory is that the ET rate does not necessarily increase with the driving force. Indeed, it is maximal when  $-\Delta G^0 = \lambda$  (the rate for this case was called free-energy optimized or optimal rate) and decreases upon further increase of  $-\Delta G^0$  in the so-called inverted region of the Marcus curve. The inverted region behavior has been experimentally demonstrated for electron transfer reactions in some organic compounds at strong driving forces ( $\lambda < -\Delta G^0 < 3\lambda$ )<sup>25–27</sup> and, for example, in ruthenium-modified cytochrome c.<sup>28</sup> For native enzymatic electron transfer, only a few cases in the inverted region have been well characterized, mostly with  $-\Delta G^0$  only slightly larger than  $\lambda$ , for example.<sup>29–32</sup>

The electronic coupling and hence the electron transfer rate decrease strongly with the distance ( $R$ ) between the donor and the acceptor. This decrease is often approximated by  $k_{\text{et}} \propto H_{\text{AB}}^2 \propto e^{-\beta R}$ , where  $\beta$  depends on the medium between the donor and the acceptor. For a number of ET reactions in purple bacterial reaction centers over edge-to-edge distances between 4.6 and 23.4 Å, the distance dependence of the free energy optimized ET rate could be well described<sup>29</sup> by  $\beta = 1.4 \text{ Å}^{-1}$ , corresponding to 1 order of magnitude decrease per 1.64 Å. More sophisticated models take into account more details of the structure of the protein, for example.<sup>33</sup>

In enzymes, a semiempirical formula has been proposed<sup>29–31,34,35</sup> for the distance and driving force dependences of downhill ET in proteins with

$$\log_{10} k_{\text{et}} = 13 - (1.2 - 0.8\rho)(R - 3.6) - 3.1((\Delta G^0 + \lambda)^2/\lambda)$$

where  $k_{\text{et}}$  is expressed in  $\text{s}^{-1}$  and  $-\Delta G^0$  and  $\lambda$  in eV,  $\rho$  is the average packing density of the medium between the donor and the acceptor, and  $R$  is the edge-to-edge distance expressed in Å. This formula is based on electron transfer rates in oxidoreductases over distances from  $\approx 4$  to  $\approx 24$  Å.<sup>35</sup> Here we characterize an example of a very long-range ( $\approx 32$  Å edge-to-edge) electron transfer in Photosystem II, the  $S_n\text{Tyr}_Z^{\bullet}Q_A^{\bullet-}$  charge recombinations at cryogenic temperatures, which very likely occur in the Marcus inverted region.

## ■ EXPERIMENTAL SECTION

The constructions of the deletion mutants from a *T. elongatus* 43-H strain that had a His<sub>6</sub>-tag on the C-terminus of CP43<sup>36</sup> have been previously described in ref 37 for the  $\Delta\text{psbA}_1\Delta\text{psbA}_2$  *T. elongatus* deletion mutant (WT\*3), in ref 15 for the  $\Delta\text{psbA}_1\Delta\text{psbA}_3$  *T. elongatus* deletion mutant (WT\*2), and in ref 38 for the  $\Delta\text{psbA}_2\Delta\text{psbA}_3$  *T. elongatus* deletion mutant (WT\*1). Cells were grown in 1 L of DTN in 3-L Erlenmeyer flasks in a rotary shaker with a CO<sub>2</sub>-enriched atmosphere at 45 °C under continuous light ( $80 \mu\text{mol}$  of photons  $\cdot \text{m}^{-2} \cdot \text{s}^{-1}$ ) until they reached an optical density (OD) close to 1.0 at 800 nm.

After harvesting by centrifugation, the cells were washed once with buffer 1 (1 M betaine, 10% glycerol, 40 mM MES, 15 mM MgCl<sub>2</sub>, 15 mM CaCl<sub>2</sub>, pH 6.5 (adjusted with NaOH)) and resuspended in the same buffer, with 0.2% (w/v) bovine serum albumin, 1 mM benzamidine, 1 mM  $\epsilon$ -aminocaproic acid, and  $\approx 50 \mu\text{g mL}^{-1}$  DNase I added to a chlorophyll concentration of  $\approx 1.5 \text{ mg Chl mL}^{-1}$ . The cells were ruptured with a French press. Unbroken cells were removed by centrifugation (3000 g, 5 min). Membranes were pelleted by centrifugation at 180000 g for 30 min at 4 °C and washed twice with buffer 1. Thylakoids ( $1 \text{ mg Chl mL}^{-1}$ , final concentration after the addition of the detergent) were treated with 0.8% (w/v) n-dodecyl- $\beta$ -maltoside ( $\beta$ -DM, Biomol, Germany) in buffer 1 supplemented with 100 mM NaCl. After  $\approx 1$  min of stirring in the dark at 4 °C the suspension was centrifuged (20 min, 170000 g) to remove the nonsolubilized material. Then, the supernatant was mixed with an equal volume of Probond resin (Invitrogen, Groningen, The Netherlands) that had been pre-equilibrated with buffer 1. The resulting slurry was transferred to an empty column. After sedimentation of the resin inside the column, the supernatant was removed. The resin was washed with buffer 2 (1 M betaine, 10% glycerol, 40 mM MES, 15 mM MgCl<sub>2</sub>, 15 mM CaCl<sub>2</sub>, 100 mM NaCl, 1 mM L-histidine, 0.03% (w/v)  $\beta$ -DM, pH 6.5) until the OD value of the eluate at  $\approx 665 \text{ nm}$  decreased below 0.05 (approximately 15 h). Then, PSII core complexes were eluted with buffer 3 (1 M betaine, 40 mM MES, 15 mM MgCl<sub>2</sub>, 15 mM CaCl<sub>2</sub>, 200 mM NaCl, 180 mM L-histidine, 0.06% (w/v)  $\beta$ -DM, pH 6.5). The eluate was then concentrated and washed in buffer 4 with 1 M betaine, 40 mM MES, 15 mM MgCl<sub>2</sub>, 15 mM CaCl<sub>2</sub>, pH 6.5, using centrifugal filter devices (Ultrafree-15, Millipore). PSII core complexes were finally resuspended in the same buffer at a Chl concentration of  $\approx 1.5 \text{ mg Chl mL}^{-1}$  and stored in liquid N<sub>2</sub> before being used. Glycerol was avoided in the final steps because its presence prevents the full detection of the split EPR signals.<sup>16–20</sup>

For the  $\text{H}_2\text{O}/\text{D}_2\text{O}$  exchange, PSII samples purified as described above were further washed in buffer 4 prepared in  $\text{D}_2\text{O}$  with dilution/concentration cycles by using centrifugal filter devices (Ultrafree-15, Millipore). The total duration for the incubation of the samples in  $\text{D}_2\text{O}$  was approximately 6–8 h. This is much longer than the time required ( $\leq 20$  min) to observe the effect of the  $\text{H}_2\text{O}/\text{D}_2\text{O}$  exchange on the  $\text{P}_{680}^{+\bullet}$  reduction by  $\text{Tyr}_Z$  and the  $\text{Tyr}_Z^{\bullet}$  reduction by the  $\text{Mn}_4\text{CaO}_5$  cluster.<sup>39,40</sup>

Cw-EPR spectra and kinetics were recorded with a Bruker Elexsys 500 X-band spectrometer equipped for He-temperature with a standard ER 4102 (Bruker) X-band resonator, an Oxford Instruments cryostat (ESR 900) and an Oxford ITC504 temperature controller. Flash illumination at room temperature was provided by a Nd:YAG laser (532 nm, 550 mJ, 8 ns Spectra Physics GCR-230–10). PSII samples at 1.1 mg of Chl  $\text{mL}^{-1}$  were loaded in the dark into quartz EPR tubes and dark-adapted for 1 h at room temperature. Then, the samples were synchronized in the  $\text{S}_1$ -state with one preflash. After a further 1 h dark-adaptation at room temperature, 0.5 mM PPBQ dissolved in dimethylsulfoxide were added. Then, 0, 1, and 3 flashes were given to the samples to induce the  $\text{S}_1$ ,  $\text{S}_2$ , and  $\text{S}_0$  states, respectively. The samples were then immediately frozen to 198 K and then transferred to 77 K. The samples were degassed at 198 K prior to the recording of the spectra. For time-resolved EPR measurements, the samples were illuminated in the EPR cavity by four flashes, spaced 100 ms apart, provided by the laser described above with an energy close to 150 mJ. In separate experiments it has been checked that decreasing the laser energy to 75 mJ had almost no effect on the amplitude of the light-induced split signals showing that 150 mJ was saturating. As shown earlier,<sup>20</sup> four flashes were required at 4.2–50 K to induce  $\geq 90\%$  of each of the three split signals.

The literature, for example,<sup>16–21,41</sup> shows that the relative proportion of the  $\text{S}_1\text{Tyr}_Z^{\bullet}\text{Q}_A^{-\bullet}$ ,  $\text{Cyt } b_{559}^{+\bullet}\text{Q}_A^{-\bullet}$  and  $(\text{Car}/\text{Chl}_Z)^{+\bullet}\text{Q}_A^{-\bullet}$  states upon illumination at 4.2 K depends on the samples and the conditions used. To our knowledge, there is not a definitive explanation for such a variation. Yet, we would like to point out that the decay of the split signals and that of  $\text{Q}_A^{-\bullet}$  are similar<sup>20,21</sup> and that, in our conditions, both the split signal and the  $\text{Q}_A^{-\bullet}$  species fully decay in the dark, whereas the  $(\text{Car}/\text{Chl}_Z)^{+\bullet}$  remained stable (see below and Supporting Information). To avoid any contribution from carotenoid and chlorophyll radicals, the kinetics were measured at the magnetic field positions indicated by the arrows in Figure 1, that is, a magnetic field value where only the split signals contribute in the experimental conditions used here. To get spectra free from carotenoid and chlorophyll radicals, they were recorded immediately after the flash illumination and then after dark adaptation at 4.2 K after the decay of the split signals, as done earlier. On this time scale, the small amount of carotenoid and chlorophyll radicals generated in a fraction of centers by the low temperature flash illumination is virtually stable (not shown, but see refs 17–19), so that the difference spectra shown in the inset of Figure 1 are attributed to  $\text{S}_n\text{Tyr}_Z^{\bullet}$ .

Formation of the  $\text{S}_1\text{Tyr}_Z^{\bullet}$  split signal was done by flash illumination of PSII centers previously synchronized at room temperature in the  $\text{S}_1$  state. To induce the  $\text{S}_2\text{Tyr}_Z^{\bullet}$  split signals, samples synchronized in the  $\text{S}_1$  state at room temperature were first illuminated by one flash given at room temperature to induce the  $\text{S}_2$  state. Then, the samples were immediately frozen at 198 K in a  $\text{CO}_2$ –ethanol bath and further illuminated with a

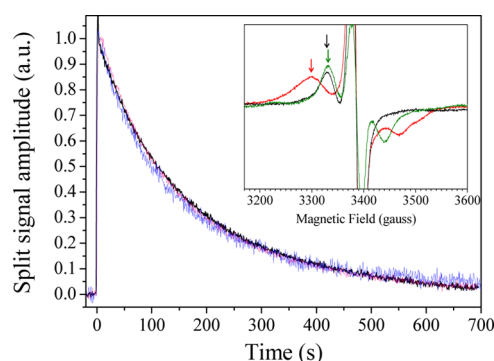


**Figure 1.** Formation and decay of the  $\text{S}_1\text{Tyr}_Z^{\bullet}$  split signal in PsbA3-PSII at 4.2 (black), 30 (red), and 50 K (blue). The traces have been normalized to the signal amplitude at 4.2 K (the signals at 30 and 50 K were amplified 1.5 and 2.9 times, respectively). The inset shows difference spectra. The first spectra were first recorded immediately after the flash illumination and the second spectra were recorded after the decay of the  $\text{S}_0\text{Tyr}_Z^{\bullet}$  (red),  $\text{S}_1\text{Tyr}_Z^{\bullet}$  (black), and  $\text{S}_2\text{Tyr}_Z^{\bullet}$  (green) split signals spectra in PsbA3-PSII. The arrows indicate the magnetic field at which the kinetics were measured. Instrument settings: modulation amplitude, 25 G; microwave power, 20 mW; microwave frequency, 9.4 GHz; modulation frequency, 100 kHz; chlorophyll concentration, 1.1 mg  $\text{mL}^{-1}$ .

continuous visible light for approximately 5 s with a 1000 W tungsten lamp filtered with water and calfix filters. After such an illumination, the  $\text{S}_2\text{Tyr}_Z^{\bullet}$  was induced but was not stable and decayed in part during the time required for the transfer of the EPR tube inside the cryostat.<sup>17–19</sup> The  $\text{S}_2\text{Tyr}_Z^{\bullet}$  split signals could then be fully induced again by illumination at helium temperatures in centers that were in the  $\text{S}_2\text{Tyr}_Z^{\bullet}$  state at 200 K.<sup>18,19</sup> In this procedure, any centers still in the  $\text{S}_1$  state after the flash illumination at room temperature due to misses were converted into  $\text{S}_2\text{Q}_A^{-\bullet}$  by the further 198 K illumination (and then are unable to reach the  $\text{S}_2\text{Tyr}_Z^{\bullet}$  state upon a further low temperature illumination) so that the split signal induced afterward at helium temperature was free from a contamination by the  $\text{S}_1\text{Tyr}_Z^{\bullet}$  split signal. To induce the  $\text{S}_0\text{Tyr}_Z^{\bullet}$  split signals, samples synchronized in the  $\text{S}_1$  state were first illuminated by three flashes at room temperature to induce the  $\text{S}_0$  state. Then, the samples were immediately frozen at 198 K in a  $\text{CO}_2$ –ethanol bath and transferred at 77 K in liquid  $\text{N}_2$  and then at 4.2 K in the EPR cryostat. In this experiments, due to the miss parameter, a percentage of centers are still in the  $\text{S}_3$  state and to a less extent in the  $\text{S}_2$  state after the illumination by three flashes. Because formation of the  $\text{S}_2\text{Tyr}_Z^{\bullet}$  split signal at helium temperature requires a preillumination at 198 K, the centers in  $\text{S}_2$  after the three flashes at room temperature did not give rise to a split signal in this experiment. The situation for centers in  $\text{S}_3$  is different because it is known that visible light illumination at liquid helium temperatures induces the formation of a  $(\text{S}_2\text{Tyr}_Z^{\bullet})'$  split signal, which is stable at 4.2 K.<sup>17–19</sup> To avoid any contribution from this  $(\text{S}_2\text{Tyr}_Z^{\bullet})'$  split signal in these centers, PSII illuminated by three flashes at room temperature were then illuminated by near-infrared illumination at 4.2 K (Coherent, diode S-81-1000C). This procedure induced the  $(\text{S}_2\text{Tyr}_Z^{\bullet})'$  split signal that is stable below 77 K. Then, in centers in the  $\text{S}_0$  state, the  $\text{S}_0\text{Tyr}_Z^{\bullet}$  split signal was induced by flash illumination.

Under the microwave power conditions used to record the split signals (20 mW), the split signals were slightly saturated at 4.2 K. In these conditions, the flash illumination at liquid



helium temperatures induced a slight warming of the samples resulting in an artifact seen as a fast increase/decrease at 4.2 K and as a fast decrease/increase above 10 K. In both cases, the lifetime of the artifact (seen as a spike at 4.2 K) was so short that it did not prevent an accurate determination of the rate constants. In all cases, the light-induced split signals fully decayed and the signals could be generated with similar amplitudes on a least five consecutive illuminations.

## RESULTS AND DISCUSSION

The EPR split signals originate from the magnetic interaction between the  $\text{Mn}_4\text{CaO}_5$  cluster and the  $\text{Tyr}_Z^\bullet$  radical in the spin  $S = 1/2$  state, for example.<sup>17,18,42–44</sup> In the  $S_1$  state and  $S_0$  state it has been shown to be induced in  $\approx 40$  and 50%, respectively, of the reaction centers.<sup>20</sup> Figure 1 shows the formation and decay kinetics of the  $S_0\text{Tyr}_Z^\bullet$ ,  $S_1\text{Tyr}_Z^\bullet$ , and  $S_2\text{Tyr}_Z^\bullet$  split signal spectra induced by laser flashes at 532 nm in PsbA3-PSII at 4.2, 30, and 50 K. The inset shows the spectra induced in PsbA3-PSII. The  $S_0\text{Tyr}_Z^\bullet$ ,  $S_1\text{Tyr}_Z^\bullet$ , and  $S_2\text{Tyr}_Z^\bullet$  split signal spectra are similar to those recorded in PsbA1-PSII (see Figure S1) and to those reported earlier in PSII from plants and cyanobacteria.<sup>16–20,42,43</sup> The arrows indicate the magnetic field values at which the time-resolved measurements reported in Figure 1 were done. Figure 1 shows that, in PsbA3-PSII, the kinetics of the  $S_1\text{Tyr}_Z^\bullet\text{Q}_A^-$  charge recombination at 4.2, 30, and 50 K were indistinguishable. The same applies to all the  $S_n\text{Tyr}_Z^\bullet\text{Q}_A^-$  charge recombination kinetics studied here. The lack of a temperature dependence of the charge recombination rules out the involvement of any thermally activated step in the overall charge recombination process, such as backward electron transfer from  $\text{Q}_A^-$  to  $\text{Pheo}_{D1}$  or from  $\text{Tyr}_Z^\bullet$  to  $\text{P}_{680}$ . Thus, the decay of the split signal arising from  $S_n\text{Tyr}_Z^\bullet\text{Q}_A^-$  most likely occurs via single step electron tunneling from  $\text{Q}_A^-$  to  $\text{Tyr}_Z^\bullet$ . In addition, these kinetics were also insensitive to H/D exchange (not shown, but see Figure S3), which indicates that a proton movement does not contribute to the energetic of the  $\text{Tyr}_Z^\bullet$  reduction when  $\text{Tyr}_Z$  is oxidized at cryogenic temperatures. These results allow the assignment of the rates experimentally determined here to pure electron transfer.

Figure 2 shows the formation and decay of the  $S_1\text{Tyr}_Z^\bullet$  (black curve) and  $S_2\text{Tyr}_Z^\bullet$  (green curve) split signals in PsbA3-PSII and of the  $S_1\text{Tyr}_Z^\bullet$  (blue curve) and  $S_2\text{Tyr}_Z^\bullet$  (red curve) split signals in PsbA1-PSII. The rate constants for the charge recombinations are indicated in Table 1. The following observations can be done: (i) Both the  $S_1\text{Tyr}_Z^\bullet\text{Q}_A^-$  and  $S_2\text{Tyr}_Z^\bullet\text{Q}_A^-$  charge recombinations were  $\approx 2$ -fold faster in PsbA3-PSII than in PsbA1-PSII, which has a lower  $E_m(\text{Q}_A/\text{Q}_A^-)$  than PsbA3-PSII, see the Introduction; (ii) in both PsbA1-PSII and PsbA3-PSII the  $S_1\text{Tyr}_Z^\bullet\text{Q}_A^-$  charge recombination was  $\approx 3$ -fold faster than the  $S_2\text{Tyr}_Z^\bullet\text{Q}_A^-$  charge recombination. Because no compensating proton release occurs upon the  $S_1$  to  $S_2$  transition, for example,<sup>45,46</sup> the electrostatic charge of the  $\text{Mn}_4\text{CaO}_5$  cluster is incremented.<sup>47</sup> As a consequence, the  $E_m(\text{Tyr}_Z^\bullet/\text{Tyr}_Z)$  value is upshifted at room temperature by  $\approx 55$  mV<sup>48</sup> in  $S_2$  when compared to  $S_1$ .

The extrapolation of figures obtained at room temperature to low temperatures should be done with cautions. However, in the present study, the different  $S_n$  states were prepared at room temperature allowing the protein moiety to relax as in the electroluminescence experiments<sup>48</sup> and as in the measurements of the  $E_m(\text{Q}_A/\text{Q}_A^-)$  values by spectroelectrochemistry,<sup>12</sup> thus, making the relative values of the driving forces meaningful in the different cases mentioned above. Therefore, it is likely that

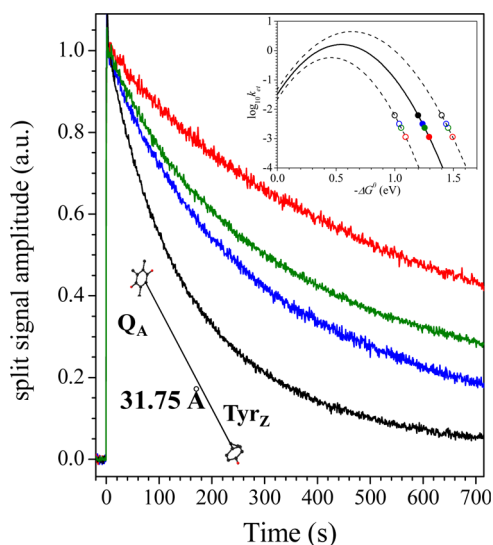


**Figure 2.** Formation and decay at 4.2 K of the  $S_n\text{Tyr}_Z^\bullet$  split signals in the various PSII: (i) in PsbA3-PSII, the  $S_1\text{Tyr}_Z^\bullet$  split signal is shown in black, the  $S_2\text{Tyr}_Z^\bullet$  split signal in green, and (ii) in PsbA1-PSII, the  $S_1\text{Tyr}_Z^\bullet$  split signal is shown in blue and the  $S_2\text{Tyr}_Z^\bullet$  split signal in red. The lower inset illustrates the edge-to-edge distance between  $\text{Tyr}_Z$  and  $\text{Q}_A^-$ . Same instrument settings as in Figure 1. The upper inset shows the driving-force dependence of electron-transfer rates and tentative fits by using the Hopfield expression with  $\hbar\omega = 70$  meV and  $T = 4.2$  K. The full symbols and the continuous line are based on a  $-\Delta G^0$  value of 1.2 eV in  $S_1$  in PsbA3-PSII. Open symbols and dashed lines are for alternative  $-\Delta G^0$  scalings (see the text). The fits resulted in the following values: For  $\Delta G^0 = -1.0$  eV,  $\lambda = 0.46$  eV and  $H_{ab} = 4.4 \times 10^{-9}$  eV. For  $\Delta G^0 = -1.2$  eV,  $\lambda = 0.55$  eV and  $H_{ab} = 7.6 \times 10^{-9}$  eV. For  $\Delta G^0 = -1.4$  eV,  $\lambda = 0.64$  eV and  $H_{ab} = 1.3 \times 10^{-8}$  eV.

upon freezing of the samples previously trapped in either  $S_1$  or  $S_2$ , the  $E_m(\text{Tyr}_Z^\bullet/\text{Tyr}_Z)$  value in  $S_2$  remains larger than in  $S_1$  and that the  $E_m(\text{Q}_A/\text{Q}_A^-)$  value in PsbA1-PSII remains lower than in PsbA3-PSII. Combining the redox changes of  $\text{Tyr}_Z$  to those of  $\text{Q}_A$ , one thus expects the driving force of the  $S_2\text{Tyr}_Z^\bullet\text{Q}_A^-$  charge recombination to be larger than that of the  $S_1\text{Tyr}_Z^\bullet\text{Q}_A^-$  charge recombination and the driving forces of the  $S_n\text{Tyr}_Z^\bullet\text{Q}_A^-$  charge recombinations to be larger in the PsbA1-PSII case than in the PsbA3-PSII one.

As recast in Table 1, in every case studied here we found that the larger the expected driving force, the smaller the rate constant. Two suggestions can be put forward here: (i) at liquid helium temperatures, the  $S_n\text{Tyr}_Z^\bullet\text{Q}_A^-$  charge recombination occurs in the inverted region of the Marcus curve and (ii) the likely rather steep dependence of the rate constant on the driving force implies that the  $-\Delta G^0$  value is much larger than  $\lambda$ . With the assumption made above that the  $\approx 38$  mV increase of the  $E_m(\text{Q}_A/\text{Q}_A^-)$  value in PsbA3-PSII when compared to PsbA1-PSII<sup>12</sup> and the  $\approx 55$  mV increase of the  $E_m(\text{Tyr}_Z^\bullet/\text{Tyr}_Z)$  value in the  $S_2$  state when compared to the  $S_1$  state<sup>49</sup> apply at cryogenic temperatures and are the only origin of the observed effects, the driving-force dependence of electron-transfer rates has been tentatively fitted by using the Hopfield equation with a fixed  $\hbar\omega = 70$  meV that was deduced from the  $\text{P}^+\text{Q}_A^-$  charge recombination kinetics at cryogenic temperatures in bacterial reaction centers.<sup>29</sup> The results are shown in the upper inset of Figure 2. First, 1.2 eV was taken for the  $-\Delta G^0$  value of the  $S_1\text{Tyr}_Z^\bullet\text{Q}_A^-$  charge recombination in PsbA3-PSII, a value close to that one estimated at room temperature.<sup>49</sup> Second, to take into account possible deviations at liquid helium

Table 1. Rate Constants for the  $S_1\text{Tyr}_Z^{\bullet}\text{Q}_A^{\bullet-}$  Charge Recombinations in PsbA1-PSII, PsbA2-PSII, and PsbA3-PSII<sup>a</sup>

PSII	PsbA1-PSII			PsbA2-PSII		PsbA3-PSII		
$S_0$	$S_0$	$S_1$	$S_2$	$S_0$	$S_1$	$S_0$	$S_1$	$S_2$
$k_{\text{et}} \text{ (s}^{-1}\text{)}$	0.0034	0.0034	0.0012	0.0058	0.0062	0.0094	0.0063	0.0020
$\gamma$	0.66	0.79	0.8	0.77	0.72	0.77	0.77	0.75

<sup>a</sup>The rate constants were estimated by fitting the data with a single stretched exponential function  $A = A_0 \exp(-(k_{\text{et}}t)^\gamma)$  (see Figure S5). Here,  $t_{1/2} = ((\ln 2)^{1/\gamma})/k_{\text{et}}$ .

temperatures, this  $-\Delta G^0$  value was set to 1.0 and 1.4 eV. The reorganization energies obtained from these fits are in the range  $0.5 \text{ eV} \leq \lambda \leq 0.7 \text{ eV}$ . The data were also fitted with other fixed vibration frequencies,  $\hbar\omega = 35$  and  $140 \text{ meV}$ , yielding  $\lambda = 0.76$  and  $0.35 \text{ eV}$ , respectively (see Figure S5). It is clear that the relatively small variation of the driving force between the four sample conditions does not allow for an accurate determination of the reorganization energy. Nevertheless, it appears that  $\lambda$  is rather small, which is not unexpected for cryogenic temperature conditions, where part of the reorganizations may be frozen.

The free-energy optimized ET rates ( $k_{\text{opt}}$ ) obtained from these fits are in the range  $0.1 \text{ s}^{-1} < k_{\text{opt}} < 10 \text{ s}^{-1}$ . This appears fast given the edge-to-edge distance of  $31.75 \text{ \AA}$  between  $\text{Q}_A$  and  $\text{Tyr}_Z$  in PSII. Extrapolating the distance dependence of ET rates in purple bacterial reaction centers (see Introduction), one would expect  $k_{\text{opt}} \approx 10^{-4} \text{ s}^{-1}$ . This deviation cannot merely stem from the uncertainties in the fitting of our data to obtain  $k_{\text{opt}}$  because already our observed rates (see Table 1) are 1–2 orders of magnitude faster than the expected  $k_{\text{opt}}$ . The low temperature in our study ( $4.2\text{--}50 \text{ K}$  compared to room temperature for the cited data on purple bacterial reaction centers) is rather expected to decrease than to increase the ET rate, except for the special case  $-\Delta G^0 = \lambda$ , but even there only a very weak increase is expected for low temperatures. Furthermore, charge recombination in the pair  $\text{P}^{+\bullet}\text{Q}_A^{\bullet-}$  in a purple bacterial reaction center (edge-to-edge distance  $R = 22.5 \text{ \AA}$ ) was studied at  $35 \text{ K}$ , yielding  $k_{\text{opt}} \approx 20 \text{ s}^{-1}$ .<sup>29</sup> Extrapolation to  $R = 31.75 \text{ \AA}$  with an exponential decay coefficient  $\beta = 1.4 \text{ \AA}^{-1}$  (see Introduction) yields an expected optimal rate of  $\approx 5 \times 10^{-4} \text{ s}^{-1}$ , again much slower than even our observed rates.

Finally, differences in the structure of the medium between donor and acceptor may account for the deviation. Page et al.<sup>30</sup> suggested to take into account the packing density ( $\rho$ ) of the protein through the simple empirical relation  $\log_{10} k_{\text{opt}} = 13 - (1.2 - 0.8\rho)(R - 3.6)$ , where  $k_{\text{opt}}$  is in  $\text{s}^{-1}$  and  $R$  in  $\text{\AA}$ . Yet, the average packing density of PSII seems to be rather similar to that of purple bacterial reaction centers.<sup>50</sup> A more detailed analysis of the electronic coupling between  $\text{Q}_A^{\bullet-}$  and  $\text{Tyr}_Z^{\bullet}$  is beyond the scope of this paper. Yet, we would like to mention that the region between  $\text{Q}_A$  and  $\text{Tyr}_Z$  contains several aromatic cofactors that might enhance the electronic coupling without being real intermediates in the  $\text{Tyr}_Z^{\bullet}\text{Q}_A^{\bullet-}$  charge recombination at cryogenic temperatures. This point may be addressed by future theoretical work. Our data might suggest that the decrease of the intraprotein electron tunneling rate with increasing distance becomes weaker at very large distances. An empirical approach to this question will have to await further experimental data on very long-range tunneling.

It has been recently proposed that the geometry of the  $\text{Tyr-O}\cdots\text{H}\cdots\text{N}\varepsilon\text{-His}$  bonding be modified in PsbA2-PSII when compared to PsbA(1/3)-PSII, and it has been shown that the consequences of this modification were much more pronounced in the  $S_2$  state than in the  $S_1$  state.<sup>15</sup> Accordingly, we found here that, at variance with the  $S_0\text{Tyr}_Z^{\bullet}$  and  $S_1\text{Tyr}_Z^{\bullet}$  split

signals that could be induced in PsbA2-PSII (although with a very slightly modified  $S_1\text{Tyr}_Z^{\bullet}$  spectrum, see Figure S1), the formation yield of the  $S_2\text{Tyr}_Z^{\bullet}$  was too low to allow its detection, at least a pH 6.5 (not shown).

Figure 3 shows the formation and then the decay kinetics at  $4.2 \text{ K}$  of the  $S_1\text{Tyr}_Z^{\bullet}$  split signals in PsbA3-PSII (black), in

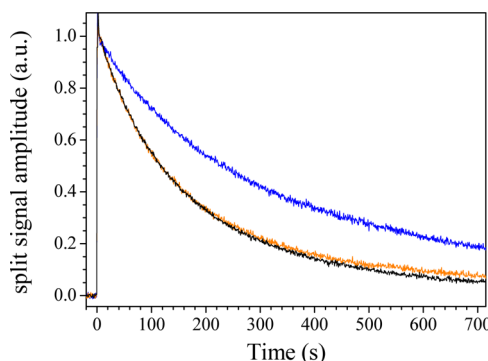


Figure 3. Formation and decay at  $4.2 \text{ K}$  of the  $S_1\text{Tyr}_Z^{\bullet}$  split signal in PsbA3-PSII (black) and of the  $S_1\text{Tyr}_Z^{\bullet}$  split signal in PsbA1-PSII (blue). The decay of the  $S_1\text{Tyr}_Z^{\bullet}$  split signal in PsbA2-PSII (orange) was found similar to that in PsbA3-PSII; same instrument settings as in Figure 2.

PsbA1-PSII (blue) and in PsbA2-PSII (orange). The latter was found similar to that in PsbA3-PSII (see also Table 1). This suggests that the driving forces of the ET reactions are similar in the  $S_1$  state in PsbA2-PSII and PsbA3-PSII. Because in the  $S_1$  state the  $\text{Tyr}_Z$  oxidation by  $\text{P}_{680}^{+\bullet}$  and the  $\text{Tyr}_Z^{\bullet}$  reduction by the  $\text{Mn}_4\text{CaO}_5$  cluster remained almost unaffected in PsbA2-PSII,<sup>15</sup> it seems likely that the  $E_m$  of the acceptor remain unchanged upon the PsbA3 to PsbA2 exchange. We thus propose that the  $E_m(\text{Q}_A/\text{Q}_A^{\bullet-})$  value in PsbA2-PSII is similar to that in PsbA3-PSII.

Because  $\approx 1$  proton is released in the oxidation of  $S_0$  into  $S_1$ ,<sup>45,46</sup>  $E_m(\text{Tyr}_Z^{\bullet}/\text{Tyr}_Z)$  is not expected to be influenced by the formation of the  $S_1$  state at the expense of  $S_0$ , and indeed, to our knowledge, there is no functional study concluding that the  $E_m(\text{Tyr}_Z^{\bullet}/\text{Tyr}_Z)$  is strongly modified upon formation of  $S_1$  at the expense of  $S_0$ . In agreement with this, the data reported in Table 1 show that the  $S_0\text{Tyr}_Z^{\bullet}\text{Q}_A^{\bullet-}$  and  $S_1\text{Tyr}_Z^{\bullet}\text{Q}_A^{\bullet-}$  charge recombination kinetics are similar in both the PsbA1-PSII and the PsbA2-PSII cases. However, in PsbA3-PSII, a small change was observed. The origin of this effect will be investigated in future works.

In this work we show that single-step electron tunneling occurs in a protein over a distance as long as  $\approx 32 \text{ \AA}$ . By using PsbA1-PSII and PsbA3-PSII with different  $E_m(\text{Q}_A/\text{Q}_A^{\bullet-})$  values, we found that the larger the driving force for the  $S_1\text{Tyr}_Z^{\bullet}\text{Q}_A^{\bullet-}$  charge recombination, the smaller the rate constant suggesting that this reaction operates in the inverted region of the Marcus curve, that is, where the driving force is

larger than the reorganization energy. The driving force at room temperature for the  $S_1\text{Tyr}_Z\cdot\text{Q}_A^-$  charge recombination has been estimated to be approximately 1.2 eV.<sup>49</sup> Assuming a similar driving force at cryogenic temperatures for the  $S_1\text{Tyr}_Z\cdot\text{Q}_A^-$  charge recombination, the data were best fitted with a reorganization energy in the order of 0.6 eV, that is,  $-\Delta G^0 \approx 2\lambda$ .

The kinetic control of charge recombination reaction by the fact that they would fall in the inverted region of the Marcus curve has been invoked in several instances. Indeed, it has been suggested that the preferential expression of PsbA3 under strong light<sup>51</sup> resulted in a more efficient direct charge recombination between the donor side and the acceptor side, thus, preventing the production of harmful  $^1\text{O}_2$  from  $^3\text{P}_{680}$  itself formed by charge recombination in the thermally repopulated  $^3[\text{P}_{680}^{+}\cdot\text{Pheo}_{\text{D1}}^{-}]$  state,<sup>52</sup> but see ref 53 for a discussion. This reasoning relied on the assumption that the charge recombination occurred in the inverted region of the Marcus curve with a  $E_m(\text{Phe}/\text{Phe}^-)$  value<sup>52</sup> and a  $E_m(\text{Q}_A/\text{Q}_A^-)$  value<sup>12</sup> higher in PsbA3-PSII than in PsbA1-PSII. The results presented here give an experimental illustration of the inverted region in Photosystem II that have remained, until now, essentially theoretical.

## ■ ASSOCIATED CONTENT

### ■ Supporting Information

EPR spectra of all the split signals are shown. The fitting procedure of the split signal decays is described. Additional data upon H/D exchange is shown. Simulations with the Hopfield equation are shown for different  $\hbar\omega$  values and for the simplified formula of Moser and Dutton. This material is available free of charge via the Internet at <http://pubs.acs.org>.

## ■ AUTHOR INFORMATION

### Corresponding Author

\*E-mail: [alain.boussac@cea.fr](mailto:alain.boussac@cea.fr). Tel.: +33 (0)1 69 08 72 06.

### Notes

The authors declare no competing financial interest.

## ■ ACKNOWLEDGMENTS

A.B. was supported in part by a CEA/DSV "Bioénergie" Grant. M.S. was supported by the JST-PRESTO program (4018).

## ■ ABBREVIATIONS

ET, electron transfer; PSII, Photosystem II; Chl, chlorophyll; MES, 2-(N-morpholino) ethanesulfonic acid;  $\text{P}_{680}$ , chlorophyll dimer acting as the second electron donor;  $\text{Q}_A$ , primary quinone acceptor;  $\text{Q}_B$ , secondary quinone acceptor; 43H, *T. elongatus* strain with a His-tag on the C terminus of CP43; EPR, electron paramagnetic resonance; PQ, plastoquinone 9; WT\*1, WT\*2, and WT\*3, cells containing only the *psbA1*, *psbA2*, and *psbA3* gene, respectively;  $\text{Pheo}_{\text{D1}}$ , pheophytin;  $\text{P}_{\text{D1}}$  and  $\text{P}_{\text{D2}}$ , Chl monomer of  $\text{P}_{680}$  on the D1 and D2 side, respectively

## ■ REFERENCES

- (1) Umena, Y.; Kawakami, K.; Shen, J.-R.; Kamiya, N. Crystal Structure of Oxygen-Evolving Photosystem II at a Resolution of 1.9 Å. *Nature* **2011**, *473*, 55–65.
- (2) Diner, B. A.; Rappaport, F. Structure, Dynamics, and Energetics of the Primary Photochemistry of Photosystem II of Oxygenic Photosynthesis. *Annu. Rev. Plant Biol.* **2002**, *53*, 551–580.

- (3) Renger, G. Mechanism of Light Induced Water Splitting in Photosystem II of Oxygen Evolving Photosynthetic Organisms. *Biochim. Biophys. Acta* **2012**, *1817*, 1164–1176.

- (4) Groot, M. L.; Pawlowicz, N. P.; vanWilderen, L. J.; Breton, J.; vanStokkum, I. H.; vanGrondelle, R. Initial Electron Donor and Acceptor in Isolated Photosystem II Reaction Centers Identified with Femtosecond Mid-IR Spectroscopy. *Proc. Natl. Acad. Sci. U.S.A.* **2005**, *102*, 13087–13092.

- (5) Holzwarth, A. R.; Muller, M. G.; Reus, M.; Nowaczyk, M.; Sander, J.; Rogner, M. Kinetics and Mechanism of Electron Transfer in Intact Photosystem II and in the Isolated Reaction Center: Pheophytin is the Primary Electron Acceptor. *Proc. Natl. Acad. Sci. U.S.A.* **2006**, *103*, 6895–6900.

- (6) Crofts, A. R.; Wraight, C. A. The Electrochemical Domain of Photosynthesis. *Biochim. Biophys. Acta* **1983**, *726*, 149–185.

- (7) Velthuys, B. R.; Ames, J. Charge Accumulation at Reducing Side of System 2 of Photosynthesis. *Biochim. Biophys. Acta* **1974**, *333*, 85–94.

- (8) Kok, B.; Forbush, B.; McGloin, M. Cooperation of Charges in Photosynthetic  $\text{O}_2$  Evolution: 1. A Linear 4-Step Mechanism. *Photochem. Photobiol.* **1970**, *11*, 457–475.

- (9) Joliot, P.; Kok, B. Oxygen Evolution in Photosynthesis. In *Bioenergetics of Photosynthesis*; Govindjee, Ed.; Academic Press: New York, 1975; pp 387–412.

- (10) Mulo, P.; Sicora, C.; Aro, E. M. Cyanobacterial *psbA* Gene Family: Optimization of Oxygenic Photosynthesis. *Cell. Mol. Life Sci.* **2009**, *66*, 3697–3710.

- (11) Nakamura, Y.; Kaneko, T.; Sato, S.; Ikeuchi, M.; Katoh, H.; Sasamoto, S.; Watanabe, A.; Iriguchi, M.; Kawashima, K.; Kimura, T.; et al. Complete Genome Structure of the Thermophilic Cyanobacterium *Thermosynechococcus elongatus* BP-1. *DNA Res.* **2002**, *9*, 123–130.

- (12) Kato, Y.; Shibamoto, T.; Yamamoto, S.; Watanabe, T.; Ishida, N.; Sugiura, M.; Rappaport, F.; Boussac, A. Influence of the PsbA1/PsbA3,  $\text{Ca}^{2+}/\text{Sr}^{2+}$  and  $\text{Cl}^-/\text{Br}^-$  Exchanges on the Redox Potential of the Primary Quinone  $\text{Q}_A$  in Photosystem II from *Thermosynechococcus elongatus* as Revealed by Spectroelectrochemistry. *Biochim. Biophys. Acta* **2012**, *1817*, 1998–2004.

- (13) Boussac, A.; Rappaport, F.; Carrier, P.; Verbavatz, J.-M.; Gobin, R.; Kirilovsky, D.; Rutherford, A. W.; Sugiura, M. Biosynthetic  $\text{Ca}^{2+}/\text{Sr}^{2+}$  Exchange in the Photosystem II Oxygen Evolving Enzyme of *Thermosynechococcus elongatus*. *J. Biol. Chem.* **2004**, *279*, 22809–22819.

- (14) Ishida, N.; Sugiura, M.; Rappaport, F.; Lai, T.-L.; Rutherford, A. W.; Boussac, A. Biosynthetic Exchange of Bromide for Chloride and Strontium for Calcium in the Photosystem II Oxygen-Evolving Enzyme. *J. Biol. Chem.* **2008**, *283*, 13330–13340.

- (15) Sugiura, M.; Ogami, S.; Kusumi, M.; Un, S.; Rappaport, F.; Boussac, A. Environment of  $\text{Tyr}_Z$  in Photosystem II from *Thermosynechococcus elongatus* in which PsbA2 Is the D1 Protein. *J. Biol. Chem.* **2012**, *287*, 13336–13347.

- (16) Zhang, C.; Styring, S. Formation of Split Electron Paramagnetic Resonance Signals in Photosystem II Suggests that Tyrosine-Z Can Be Photooxidized at 5 K in the S-0 and S-1 States of the Oxygen-Evolving Complex. *Biochemistry* **2003**, *42*, 8066–8076.

- (17) Havelius, K. G. V.; Sjöholm, J.; Ho, F. M.; Mamedov, F.; Styring, S. Metalloradical EPR Signals from the  $\text{Y}_Z^\bullet$  S-State Intermediates in Photosystem II. *Appl. Magn. Reson.* **2012**, *37*, 151–176.

- (18) Petrouleas, V.; Koulougliotis, D.; Ioannidis, N. Trapping of Metalloradical Intermediates of the S-states at Liquid Helium Temperatures. Overview of the Phenomenology and Mechanistic Implications. *Biochemistry* **2005**, *44*, 6723–6728.

- (19) Boussac, A.; Sugiura, M.; Lai, T.-L.; Rutherford, A. W. Low-Temperature Photochemistry in Photosystem II from *Thermosynechococcus elongatus* Induced by Visible and Near-Infrared Light. *Philos. Trans. R. Soc.* **2008**, *363*, 1203–1210.

- (20) Zhang, C. X.; Boussac, A.; Rutherford, A. W. Low-Temperature Electron Transfer in Photosystem II: A Tyrosyl Radical and Semiquinone Charge Pair. *Biochemistry* **2004**, *43*, 13787–13795.



- (21) Cox, N.; Ho, F. M.; Pevnim, N.; Steffen, R.; Smith, P. J.; Havelius, K. G. V.; Hughes, J. L.; Debono, L.; Styring, S.; Krausz, E.; Pace, R. J. The S-1 Split Signal of Photosystem II; a Tyrosine-Manganese Coupled Interaction. *Biochim. Biophys. Acta* **2009**, *1787*, 882–889.
- (22) Marcus, R. A. Chemical + Electrochemical Electron-Transfer Theory. *Annu. Rev. Phys. Chem.* **1964**, *15*, 155–196.
- (23) Marcus, R. A.; Sutin, N. Electron Transfers in Chemistry and Biology. *Biochim. Biophys. Acta* **1985**, *811*, 265–322.
- (24) Hopfield, J. J. Electron-Transfer Between Biological Molecules by Thermally Activated Tunneling. *Proc. Natl. Acad. Sci. U.S.A.* **1974**, *71*, 3640–3644.
- (25) Miller, J. R.; Beitz, J. V.; Huddleston, R. K. Effect of Free-Energy on Rates of Electron-Transfer Between Molecules. *J. Am. Chem. Soc.* **1984**, *106*, 5057–5068.
- (26) Closs, G. L.; Calcaterra, L. T.; Green, N. J.; Penfield, K. W.; Miller, J. R. Distance, Stereoelectronic Effects, and the Marcus Inverted Region in Intramolecular Electron-Transfer in Organic Radical-Anions. *J. Phys. Chem.* **1986**, *90*, 3673–3683.
- (27) Closs, G. L.; Miller, J. R. Intramolecular Long-Distance Electron-Transfer in Organic Molecules. *Science* **1988**, *240*, 440–447.
- (28) Mines, G. A.; Bjerrum, M. J.; Hill, M. G.; Casimiro, D. R.; Chang, I.-J.; Winkler, J. R.; Gray, H. B. Rates of Heme Oxidation and Reduction in Ru(His33) Cytochrome c at Very High Driving Forces. *J. Am. Chem. Soc.* **1996**, *118*, 1961–1965.
- (29) Moser, C. C.; Keske, J. M.; Warncke, K.; Farid, R. S.; Dutton, P. L. Nature of Biological Electron-Transfer. *Nature* **1992**, *355*, 796–802.
- (30) Page, C. C.; Moser, C. C.; Chen, X.; Dutton, P. L. Natural Engineering Principles of Electron Tunneling in Biological Oxidation-Reduction. *Nature* **1999**, *402*, 47–52.
- (31) Moser, C. C.; Dutton, P. L. *Protein Electron Transfer In Outline of Theory of Protein Electron Transfer*; Bendal, D. S., Ed.; BIOS Scientific Publishers Ltd.: Oxford, 1996; pp 1–21.
- (32) Gunner, M. R.; Dutton, P. L. Temperature and  $\Delta G^0$ -Dependence of the Electron-Transfer from BPh<sup>-</sup> to Q<sub>A</sub> in Reaction Center Protein from *Rhodobacter sphaeroides* with Different Quinones as Q<sub>A</sub>. *J. Am. Chem. Soc.* **1989**, *111*, 3400–3412.
- (33) Warren, J. J.; Ener, M. E.; Vlcek, A.; Winkler, J. R.; Gray, H. B. Electron Hopping through Proteins. *Coord. Chem. Rev.* **2012**, *256*, 2478–2487.
- (34) Moser, C. C.; Anderson, J.-L.; Dutton, P. L. Guidelines for Tunneling in Enzymes. *Biochim. Biophys. Acta* **2010**, *1797*, 1573–1586.
- (35) Moser, C. C.; Page, C. C.; Dutton, P. L. Tunneling in PSII. *Photochem. Photobiol. Sci.* **2005**, *4*, 933–939.
- (36) Sugiura, M.; Inoue, Y. Highly Purified Thermo-Stable Oxygen-Evolving Photosystem II Core Complex from the Thermophilic Cyanobacterium *Synechococcus elongatus* Having His-Tagged CP43. *Plant Cell Physiol.* **1999**, *40*, 1219–1231.
- (37) Sugiura, M.; Boussac, A.; Noguchi, T.; Rappaport, F. Influence of Histidine-198 of the D1 Subunit on the Properties of the Primary Electron Donor, P<sub>680</sub>, of Photosystem II in *Thermosynechococcus elongatus*. *Biochim. Biophys. Acta* **2008**, *1777*, 331–342.
- (38) Ogami, S.; Boussac, A.; Sugiura, M. Deactivation Processes in PsbA1-Photosystem II and PsbA3-Photosystem II under Photo-inhibitory Conditions in the Cyanobacterium *Thermosynechococcus elongatus*. *Biochim. Biophys. Acta* **2012**, *1817*, 1322–1330.
- (39) Schilstra, M. J.; Rappaport, F.; Nugent, J. H. A.; Barnett, C. J.; Klug, D. R. Proton/Hydrogen Transfer Affects the S-State-Dependent Microsecond Phases of P<sub>680</sub><sup>+</sup> Reduction During Water Splitting. *Biochemistry* **1998**, *37*, 3974–3981.
- (40) Haumann, M.; Bogershausen, O.; Cherepanov, D.; Ahlbrink, R.; Junge, W. Photosynthetic Oxygen Evolution: H/D Isotope Effects and the Coupling Between Electron and Proton Transfer During the Redox Reactions at the Oxidizing Side of Photosystem II. *Photosynth. Res.* **1997**, *51*, 193–208.
- (41) Bao, H.; Zhang, C. X.; Ren, Y. N.; Zhao, J. Q. Low-Temperature Electron Transfer Suggests Two Types of Q<sub>A</sub> in Intact Photosystem II. *Biochim. Biophys. Acta* **2010**, *1797*, 339–346.
- (42) Boussac, A.; Zimmermann, J.-L.; Rutherford, A. W.; Lavergne, J. Histidine Oxidation in the Oxygen-Evolving Photosystem-II Enzyme. *Nature* **1990**, *347*, 303–306.
- (43) Koulougliotis, D.; Teutloff, C.; Sanakis, Y.; Lubitz, W.; Petrouleas, V. The S<sub>1</sub>Y<sub>Z</sub><sup>\*</sup> Metalloradical Intermediate in Photosystem II: An X- and W-band EPR Study. *Phys. Chem. Chem. Phys.* **2004**, *6*, 4859–4863.
- (44) Un, S.; Boussac, A.; Sugiura, M. Characterization of the Tyrosine-Z Radical and Its Environment in the Spin-Coupled S<sub>2</sub>Tyr<sub>Z</sub><sup>\*</sup> State of Photosystem II from *Thermosynechococcus elongatus*. *Biochemistry* **2007**, *46*, 3138–3150.
- (45) Suzuki, H.; Sugiura, M.; Noguchi, T. Monitoring Proton Release During Photosynthetic Water Oxidation in Photosystem II by Means of Isotope-Edited Infrared Spectroscopy. *J. Am. Chem. Soc.* **2009**, *131*, 7849–7857.
- (46) Rappaport, F.; Lavergne, J. Proton Release During Successive Oxidation Steps of the Photosynthetic Water Oxidation Process: Stoichiometries and pH-Dependence. *Biochemistry* **1991**, *30*, 10004–10012.
- (47) Rappaport, F.; Lavergne, J. Coupling of Electron and Proton Transfer in the Photosynthetic Water Oxidase. *Biochim. Biophys. Acta* **2001**, *1503*, 246–259.
- (48) Vos, M. H.; vanGorkom, H. J.; vanLeeuwen, P. J. An Electroluminescence Study of Stabilization Reactions in the Oxygen-Evolving Complex of Photosystem-II. *Biochim. Biophys. Acta* **1991**, *1056*, 27–39.
- (49) Rappaport, F.; Diner, B. A. Primary Photochemistry and Energetics Leading to the Oxidation of the Mn<sub>4</sub>Ca Cluster and to the Evolution of Molecular Oxygen in Photosystem II. *Coord. Chem. Rev.* **2008**, *252*, 259–272.
- (50) Moser, C. C.; Page, C. C.; Chen, X.; Dutton, P. L. Biological Electron Tunneling Through Native Protein Media. *J. Biol. Inorg. Chem.* **1997**, *2*, 393–398.
- (51) Sander, J.; Nowaczyk, M.; Buchta, J.; Dau, H.; Vass, I.; Deák, Z.; Dorogi, M.; Iwai, M.; Rögner, M. Functional Characterization and Quantification of the Alternative *psbA* Copies in *Thermosynechococcus elongatus* and Their Role in Photoprotection. *J. Biol. Chem.* **2010**, *285*, 29851–29856.
- (52) Kós, P. B.; Deak, Z.; Cheregi, O.; Vass, I. Differential Regulation of *psbA* and *psbD* Gene Expression, and the Role of the Different D1 Protein Copies in the Cyanobacterium *Thermosynechococcus elongatus* BP-1. *Biochim. Biophys. Acta* **2008**, *1777*, 74–83.
- (53) Rutherford, A. W.; Osyczka, A.; Rappaport, F. Back-Reactions, Short-Circuits, Leaks and Other Energy Wasteful Reactions in Biological Electron Transfer: Redox Tuning to Survive Life in O<sub>2</sub>. *FEBS Lett.* **2012**, *586*, 603–616.